

Article

Steel Slag Decorated with Calcium Oxide and Cerium Oxide as a Solid Base for Effective Transesterification of Palm Oil

Jichao Sun ¹, Hewei Yu ^{1,*}, Peisen Zhang ¹, Gaoyu Qi ¹, Xiuxiu Chen ², Xiaohui Liang ² and Hongyu Si ^{2,*}

¹ School of Energy and Power Engineering, Qilu University of Technology (Shandong Academy of Sciences), Jinan 250353, China

² Energy Research Institute, Qilu University of Technology (Shandong Academy of Sciences), Jinan 250013, China

* Correspondence: yhw@qlu.edu.cn (H.Y.); sihyusderi@163.com (H.S.)

Abstract: For further resource utilization of solid waste steel slag and the reduction in biodiesel production costs, this study used steel slag as a carrier to synthesize a CaO-CeO₂/slag solid base catalyst for the effective transesterification of palm oil into fatty acid methyl esters (FAMEs). The synthesis involved a two-step impregnation of steel slag with nitrate of calcium and cerium and thermal activation at 800 °C for 180 min. Then, the catalysts' textural, chemical, and CO₂ temperature-programmed desorption properties were characterized. The catalytic activity depended highly on the ratio of Ca-Ce to steel slag mass; the CaO-CeO₂/slag-0.8 catalyst showed outstanding performance. Characterization showed that the surface area and total basicity of the Ca-Ce/slag-0.8 catalyst were 3.66 m²/g and 1.289 mmol/g, respectively. The reactivity results showed that FAMEs obtained using 7 wt.% catalyst, 9:1 of methanol-to-palm-oil molar ratio, 180 min reaction duration, and 70 °C reaction temperature was optimum (i.e., 95.3% yield). In addition, the CaO-CeO₂/slag-0.8 catalyst could be reused for at least three cycles, retaining 91.2% of FAMEs yield after n-hexane washing. Hence, the catalyst exhibits an excellent potential for cost-effective and environmentally friendly biodiesel production.

Keywords: steel slag; calcium oxide; cerium oxide; transesterification; biodiesel



Citation: Sun, J.; Yu, H.; Zhang, P.; Qi, G.; Chen, X.; Liang, X.; Si, H. Steel Slag Decorated with Calcium Oxide and Cerium Oxide as a Solid Base for Effective Transesterification of Palm Oil. *Processes* **2023**, *11*, 1810. <https://doi.org/10.3390/pr11061810>

Academic Editor: Aldo Muntoni

Received: 22 May 2023

Revised: 7 June 2023

Accepted: 12 June 2023

Published: 14 June 2023



Copyright: © 2023 by the authors. Licensee MDPI, Basel, Switzerland. This article is an open access article distributed under the terms and conditions of the Creative Commons Attribution (CC BY) license (<https://creativecommons.org/licenses/by/4.0/>).

1. Introduction

The energy shortage and pollutant emission crisis have prompted researchers to develop new energy sources to replace traditional fossil fuels. Biofuel refers to solid, liquid, or gas fuel made of or extracted from biomass, and is an essential direction in developing and using renewable energy. Biodiesel has become one of the clean energy substitutes for ordinary petrochemical diesel because of its reproducibility, high calorific value, and environmental friendliness. Biodiesel is chemically classified as fatty acid methyl esters (FAMEs) [1]. It is usually obtained by the transesterification of triglycerides (e.g., vegetable oil, animal fat, microalgae oil, and waste oil) and alcohol (typically methanol) in the presence of a catalyst (Figure 1) [2].

Catalysis is crucial to biodiesel technology. Homogeneous acid and base catalysts have high catalytic efficiencies, but they portend recycling and pH-neutral wastewater challenges. Solid acid catalysts can synergistically catalyze the esterification and transesterification of waste oil. However, they usually require a much higher reaction temperature or longer reaction time. Solid base catalysts are easy to separate, and the transesterification conditions are mild, conducive to biodiesel's continuous and large-scale sustainable production with in-depth research value.

Several types of solid bases (such as alkali earth metal oxides, alkali metal-supported catalysts, solid base catalysts supported by molecular sieves, hydrotalcite, anion-exchange resins, and so on) can be used in transesterification catalysis to prepare biodiesel [3]. Popular among them are the alkaline earth metal oxides (such as CaO, MgO, SrO, and BaO). They

are solid base catalysts whose basic sites mainly come from oxygen with negative electric lattice and hydroxyl group generated by water adsorption on the surface. CaO is considered one of the most promising solid base catalysts for biodiesel production due to its high basicity, availability, and economy. Yaşar et al. [4] used CaO derived from calcinated waste eggshell to catalyze rapeseed oil and methanol under the optimized reaction conditions of 4% catalyst, 1 h reaction time at 60 °C, to achieve 95.12% biodiesel yield. However, in the reaction system with only a CaO catalyst, the leaching of Ca^{2+} species into the reaction media was a crucial problem affecting the stability of the catalyst [5]. Pandit et al. [6] confirmed that in the catalytic transesterification of microalgal oil and methanol by CaO catalyst, Ca^{2+} leaching would reduce the availability of the active site of reactants, reducing the conversion from 89.7% to 78.2% after three cycles.

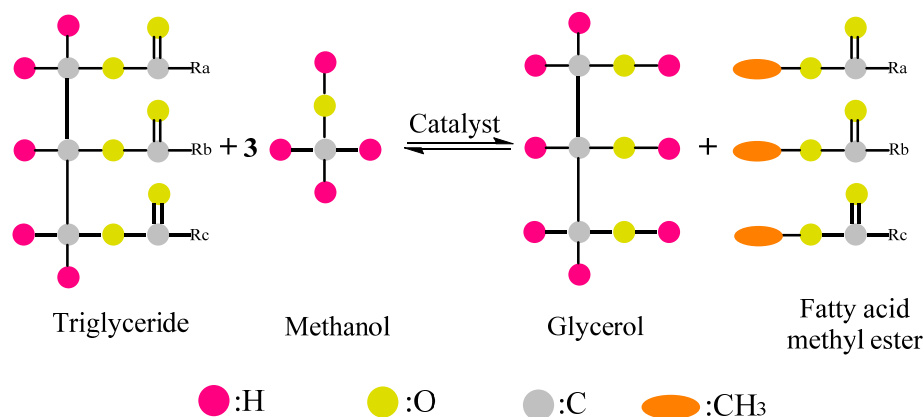


Figure 1. Schematic diagram of transesterification reaction.

Currently, CeO_2 is the most widely used rare earth metal oxide, capable of forming oxygen vacancies. It has excellent catalytic oxidation performance due to its unique crystal structure and high capacity for storing and releasing oxygen. Meanwhile, Ce exhibits acid-base dual properties, which can improve the catalyst's stability. Dehghani et al. [7] synthesized an active and stable catalyst of CaO-loaded Ce-MCM-41 to transform waste vegetable oil into biodiesel. A 96.8% conversion of triglycerides can be achieved at a methanol-to-oil molar ratio of 9 with 5 wt.% of catalyst loading at 60 °C and for 6 h. Elsewhere, Zhang et al. [8] prepared a novel $\text{CeO}_2@CaO$ catalyst via a hydrothermal method, achieving 98% biodiesel yield after 6 h. Repeated tests indicated that >80% of biodiesel yield could be obtained after nine reaction cycles, establishing the stability of $\text{CeO}_2@CaO$. These studies showed that catalyst stability could be improved after complexing CaO with CeO_2 . Yet, the catalytic activity of this catalyst type should be further optimized to shorten the reaction time.

China is the leading steel producer and supplier nation, accounting for over half of the global steel production [9]. As a by-product of steel production, steel slag accounts for 10–20% of crude steel. China's annual output of steel slag is about 70 million tons; the cumulative inventory exceeds 1 billion tons, and the utilization rate of steel slag is only about 30% [10]. Unutilized steel slag occupies a large amount of industrial land and causes excellent pressure on the atmosphere, soil, and water. Therefore, seeking comprehensive utilization of steel slag conforms to the requirement of sustainable development. Additionally, it is a basis for developing a circular economy and building green homes.

The steel slag contains majorly CaO, SiO_2 , Al_2O_3 , MnO, MgO, Fe_2O_3 , P_2O_5 , and free calcium oxide (f-CaO) [11]. For resource utilization of steel slag, Liu et al. [12] studied the synthesis of hydrotalcite-type mixed oxide catalysts from waste steel slag for transesterification. Casiello et al. [13] verified the feasibility of steel slag as a catalyst for synthesizing fumes from soybean oil. Elsewhere, Kang et al. [14] prepared a novel CeO_2 -loaded porous alkali-activated steel slag-based photocatalyst used for photocatalytic water-splitting for hydrogen production. Lin et al. [15] used acid leaching–electrolyzation–calcination to treat

steel slag in preparing catalytic H₂O₂ degradation of dye wastewater as a catalyst. The above studies fully demonstrated the effective use of steel slag in catalyst research.

The present study introduced steel slag as a carrier to combine the active components of CaO and CeO₂ to prepare a solid base catalyst. We investigated the effect of the mass ratio of CaO-CeO₂ to steel slag on the catalytic performance of CaO-CeO₂/slag catalysts. Various technologies, including N₂ adsorption-desorption, X-ray diffraction (XRD), X-ray photoelectron spectroscopy (XPS), field-emission scanning electron microscopy coupled with energy-dispersive spectroscopy (SEM-EDS), Fourier-transform infrared spectroscopy (FTIR), and CO₂-temperature-programmed desorption (TPD) clarified the physical and chemical properties of the catalysts. Reaction parameters (such as catalyst dosage, methanol-to-oil molar ratio, reaction temperature, and duration) were optimized for catalytic transesterification to achieve the highest biodiesel yield. Finally, the acid resistance and reusability of the CaO-CeO₂/slag catalyst were conducted to evaluate the catalyst's feasibility for biodiesel production.

2. Materials and Methods

2.1. Materials

The analytical grade reagents of cerium(III) nitrate hexahydrate (Ce(NO₃)₃·6H₂O) (>99.0% purity), calcium(II) nitrate tetrahydrate (Ca(NO₃)₂·4H₂O) (>98.5% purity), anhydrous methanol (>99.5% purity), anhydrous ethanol (>99.7% purity) were purchased from Sinopharm Chemical Reagent Co. Ltd. (Shanghai, China). The chromatographic grade reagents n-hexane (>99.9% purity) and methyl salicylate (>99.5% purity) were supplied by Aladdin Reagent Co., Ltd. (Shanghai, China).

Steel slag was collected from a steel mill at Yanshan City located in Hebei Province, China. The chemical composition of the original steel slag (Table 1) was analyzed by X-ray fluorescence (XRF). The palm oil was procured from Guangdong Province, China, which was native to Malaysia. Its compositions were quantitatively analyzed with myristic acid (C14:0, 1.2%), palmitic acid (C16:0, 39.51%), lauric acid (C17:0, 0.27%), stearic acid (C18:0, 7.8%), arachidic acid (C20:0, 0.33%), oleic acid (C18:1, 39.71%), and linoleic acid (C18:2, 11.13%). Its acid value (AV) and saponification value (SV), seen in Table 2, were determined through GB 5009.229-2016 and GB/T 5534-2008 criteria, respectively. Besides, the palm oil's average relative molecular weight (*M*, g/mol) can be estimated using Equation (1).

$$M = \frac{1000 \times 3 \times 56.1}{SV - AV} \quad (1)$$

Table 1. Chemical composition of the original steel slag/%.

CaO	SiO ₂	Al ₂ O ₃	MgO	SO ₃	TiO ₂	P ₂ O ₅	Fe ₂ O ₃	MnO	K ₂ O	Na ₂ O	Other
41.36	31.09	13.34	8.85	2.30	1.11	0.40	0.38	0.36	0.34	0.34	0.13

Table 2. Basic indices of the palm oil used in the current study.

Reagent	AV mgKOH/g	SV mgKOH/g	<i>M</i> g/mol
Palm oil	0.42	182.60	923.98

2.2. Catalyst Synthesis and Evaluation of Activity

The steel slag was ground into a fine powder using a pulverizer, and sieved using a 125 µm standard sieve. Ca(NO₃)₂·4H₂O and Ce(NO₃)₃·6H₂O, which provided the active site components, and the steel slag as their carriers were successively dissolved in deionized water in a particular proportion and impregnated at room temperature for 120 min using a magnetic agitator. After soaking, it was dried in a water bath at 90 °C. Afterward, the dried catalyst precursors were placed in a muffle furnace and heated to 800 °C for 180 min at a

5 °C/min heating rate to obtain the Ca-Ce/slag- x catalyst. Here, x represents the mass ratio of CaO to steel slag, calculated from the mass of $\text{Ca}(\text{NO}_3)_2 \cdot 4\text{H}_2\text{O}$. During the experiment, x was 0.4, 0.6, 0.8, and 1.0. Here, the mass ratio of CaO to CeO_2 was fixed at 1:1.

The synthesized Ca-Ce/slag- x catalyst catalyzed the transesterification of palm oil and methanol, and the catalytic activity was evaluated. The entire experimental flow chart is exhibited in Figure 2. A total of 20 g of palm oil was first poured into a 250 mL three-necked flask. Then, the Ca-Ce/slag- x catalyst and methanol (in proportion to palm oil) were transferred to the flask. The reaction flask was placed in the microwave reactor. A thermocouple was inserted to measure the reaction temperature, while magnetic stirring ensured the homogeneity of the reactants. After the transesterification, the Ca-Ce/slag- x catalyst and liquid products were separated via centrifugation. The liquid products were transferred into a separatory funnel to realize the layering of crude biodiesel and glycerin. Then, the crude biodiesel was dried at 105 °C to remove the unreacted methanol before gas chromatographic (GC) analysis.

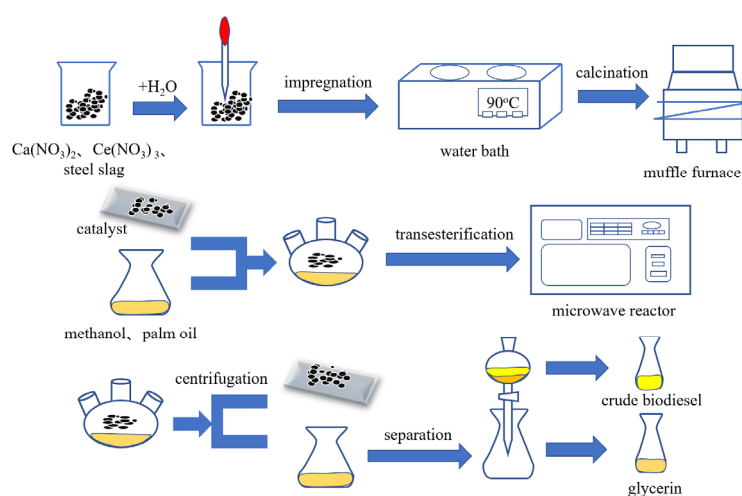


Figure 2. The experimental flow chart of catalyst synthesis and transesterification.

The FAMES were assessed using an 8890 gas chromatograph (Agilent, California, USA) equipped with a flame ionization detector (FID) and an HP-5 (30 m \times 320 μm \times 0.25 μm) column and determined by internal standardization. n-hexane was the solvent used to prepare the GC sample, while methyl salicylate served as the internal standard. The injector and FID temperatures were 250 and 300 °C, respectively. The programmed temperature of the column oven was set as follows: start at 140 °C (keep for 4 min) and ramp at 10 °C/min to 260 °C (keep for 12 min). High-purity nitrogen was the carrier gas with a split ratio of 25:1. FAMES' yield of the products was analyzed according to the reference method with methyl salicylate, and calculated using the following Equation (2) [16]:

$$\text{FAMES' yield}(\%) = \frac{\sum f_{\text{ester}} A_{\text{ester}}}{A_{\text{internal}}} \times \frac{m_{\text{internal}}}{m_{\text{sample}}} \times 100\% \quad (2)$$

where A_{ester} is the peak area of FAME, A_{internal} is the peak area of internal standard, m_{internal} is the mass of methyl salicylate, m_{sample} is the mass of the sample used, and f_{ester} is the correction factor of the FAME.

2.3. Catalyst Characterization

The XPS analyses were carried out on a Thermo escalab 250Xi (Thermo Fisher, Waltham, MA, USA) with Al $K\alpha$ radiation ($h\nu = 1486.6$ eV). The test results were corrected with C1s as 284.8 eV. Further, XRD spectra were obtained using a SmartLab apparatus (Rigaku, Tokyo, Japan) to investigate the crystalline phases in the 2θ range from 5° to 90° with a step size of 0.02° and at a scanning speed of 5°/min. The tube voltage and electricity

current were 40 kV and 30 mA, respectively. Additionally, the average crystalline size of the catalyst was evaluated using the Debye–Scherrer equation, expressed as $D = K\gamma/\beta\cos\theta$, where K is the Scherrer constant, γ is the wavelength of the X-ray, β is the half-peak width of the diffraction peak of the measured sample, and θ is the Bragg angle. The catalyst's morphology was inspected by SUPRA™ 55 FE-SEM (Zeiss, Oberkochen, Germany) with an accelerating voltage of 5 kV. Additionally, the elemental distribution of the catalyst was synchronously detected by the EDS instrument. Here, the sample was sprayed with Au to enhance its electrical conductivity. In addition, the textural properties of the catalyst were determined by N₂ adsorption and desorption using ASAP 2460 surface area and a porosity analyzer (Micromeritics, Norcross, Georgia, USA) at -196 °C. Before the adsorption test, the sample was degassed at 100 °C for 3 h under a vacuum. The Brunauer–Emmer–Teller (BET) absorption curve and the Barrett–Joyner–Halenda (BJH) model determined the catalyst's surface area and pore size distribution. The FTIR spectroscopy evaluated the functional groups of the catalyst on an iS50/6700 spectrometer (Thermo Fisher Scientific, Waltham, MA, USA) with a wavenumber of 400 to 4000 cm⁻¹. The basic strength and basicity of the catalysts were quantitated by CO₂-TPD, using a TP-5080 (Xianquan, Tianjin, China) chemical adsorption instrument. Briefly, helium gas (pre-treated) first purged the sample at 300 °C (ramping rate of 10 °C/min) for 60 min before lowering it to 50 °C. Then, the carrier/reference gas was switched to CO₂ and adsorbed at a flow rate of 30 mL/min for 30 min before the carrier gas was switched back to helium at 50 °C for 60 min. After the baseline was stabilized, the temperature was raised to 900 °C at 10 °C/min. Ten signals were recorded every 1 s.

3. Results

3.1. Optimization of the Ca-Ce/Slag Catalyst Synthesis

We studied the effect of the Ca-Ce-to-slag mass ratio on the catalytic capability of the Ca-Ce/slag- x in the transesterification of palm oil and methanol under the following conditions: catalyst dosage = 7 wt.%, methanol-to-oil molar ratio = 15, reaction temperature = 65 °C, and reaction duration = 120 min. The results are illustrated in Figure 3. No FAMES' yield was obtained when steel slag was used as catalyst. A 36.7% FAMES' yield was only attained when the Ca-Ce-to-slag mass ratio was 0.4, probably due to insufficient active component content on the catalyst surface, leading to poor catalytic activity. When the mass ratio increased from 0.6 to 0.8, the FAMES' yield gradually optimized (from 55.0%) to 85.2%, attributed to available basic sites for transesterification. However, the yield reduced significantly to 76.2% when the mass ratio was >0.8. This occurrence may be due to excess CaO and CeO₂ agglomeration and the tethering of active sites onto clusters. Thus, the Ca-Ce/slag-1.0 catalytic performance was severely hindered [17]. Borah et al. [18] also observed excess loading of Zn on CaO, which decreased the conversion because of the structural distortion of the parent catalyst. Thus, the 0.8 mass ratio of Ca-Ce-to-slag was selected as optimum for the catalyst synthesis.

3.2. Catalyst Characterization

3.2.1. XRD Analysis

The XRD patterns of slag and Ca-Ce/slag- x catalysts are shown in Figure 4. The slag shows a considerably broad peak at 2θ of 20–40°, ascribed to aromatic carbon sheets [19], indicating the presence of uncombined carbon. For the Ca-Ce/slag- x catalysts, the peaks at $2\theta = 32.18^\circ, 37.34^\circ, 53.84^\circ, 64.12^\circ, 67.34^\circ,$ and 79.62° are attributable to the crystal faces of (111), (200), (220), (311), (222), and (400) for CaO, whereas the peaks at $2\theta = 28.52^\circ, 33.08^\circ, 47.48^\circ, 56.30^\circ, 59.06^\circ, 69.36^\circ, 76.68^\circ, 79.00^\circ,$ and 88.42° are assigned to the crystal faces of (111), (200), (220), (311), (222), (400), (331), (420), and (422) for CeO₂ [20]. We observed that the diffraction peak intensity of CaO and CeO₂ increased correspondingly with the Ca and Ce loading. Moreover, using the Debye–Scherrer equation, the average crystalline sizes of CaO and CeO₂ in the catalyst were calculated as 55.63, 63.41, 69.89, and 14.01, 14.98, 16.47 nm for the Ca-Ce/slag-0.4 catalyst, Ca-Ce/slag-0.6, and Ca-Ce/slag-1.0 catalysts,

respectively. The small average crystalline size enhances the specific surface area and pore volume of the catalyst, thus guaranteeing the catalytic activity. For the Ca-Ce/slag-1.0 catalyst, numerous accumulations, and agglomerations of CaO and CeO₂ resulted in a large average crystalline size, explaining the excessive addition of active Ca and Ce components that lowered the catalyst's activity (Figure 3).

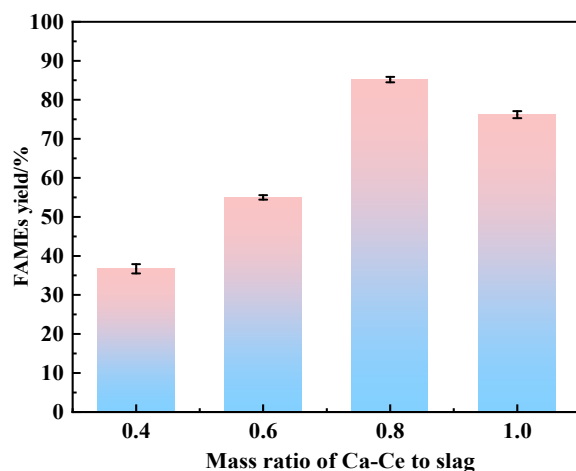


Figure 3. Effect of Ca-Ce-to-slag mass ratio.

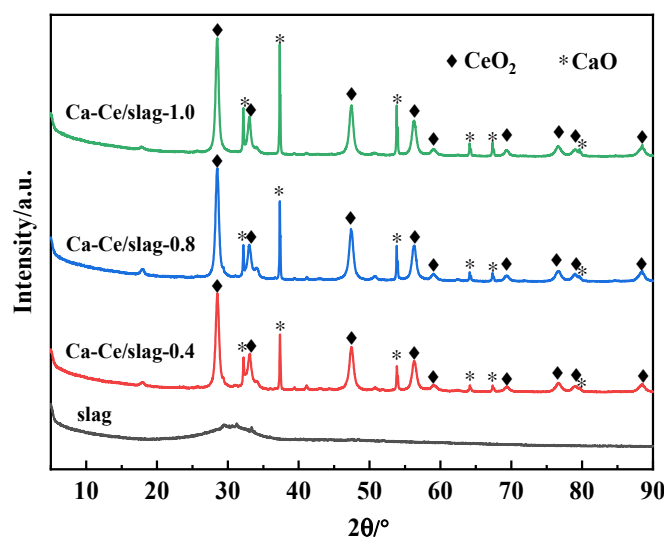


Figure 4. XRD patterns of the slag and Ca-Ce/slag-*x* catalysts.

3.2.2. N₂ Adsorption–Desorption Analysis

The microstructural properties of the slag and Ca-Ce/slag-*x* catalysts are listed in Table 3. The BET surface area of the slag, Ca-Ce/slag-0.4, and Ca-Ce/slag-0.8 catalysts are 0.27, 1.29, and 3.66 m²/g, respectively. These values indicate that CaO and CeO₂ determine the BET surface area of the catalysts within a specific numerical range. Moreover, the pore volume for the slag, Ca-Ce/slag-0.4, and Ca-Ce/slag-0.8 catalysts are 0.00049, 0.022, and 0.043 cm³/g, respectively. In general, the microstructural properties of Ca-Ce/slag-*x* are superior to those of the steel slag carrier. However, those of Ca-Ce/slag-0.8 are better than Ca-Ce/slag-0.4 catalyst, especially the average pore diameter (39.27 nm for the former; 22.19 nm for the latter). The molecular size of typical triglycerides is 5 nm [21]; hence, larger average pore sizes are more conducive to their transportation, providing better accessibility to the catalysts' active sites and favoring transesterification. The N₂ adsorption–desorption curve and pore size distribution plot of the Ca-Ce/slag-0.8 catalyst are depicted in Figure 5.

The catalyst exhibits a type V isotherm, having H3-type hysteresis loops, confirming the slit formed by the accumulation of flake particles [22]. The pore size distribution of the Ca-Ce/slag-0.8 extends from 10 to 100 nm, showing the predominance of mesopores (2–50 nm) and macropores (>50 nm). As previously established, these pore size distributions could be crucial to the catalytic biodiesel production process, conducive to mass transfer and diffusion [23].

Table 3. Microstructural properties of the slag and Ca-Ce/slag-*x* catalysts.

Samples	BET Surface Area (m ² /g)	Pore Volume (cm ³ /g)	Average Pore Diameter (nm)
slag	0.27	0.00049	-
Ca-Ce/slag-0.4	1.29	0.022	22.19
Ca-Ce/slag-0.8	3.66	0.043	39.27

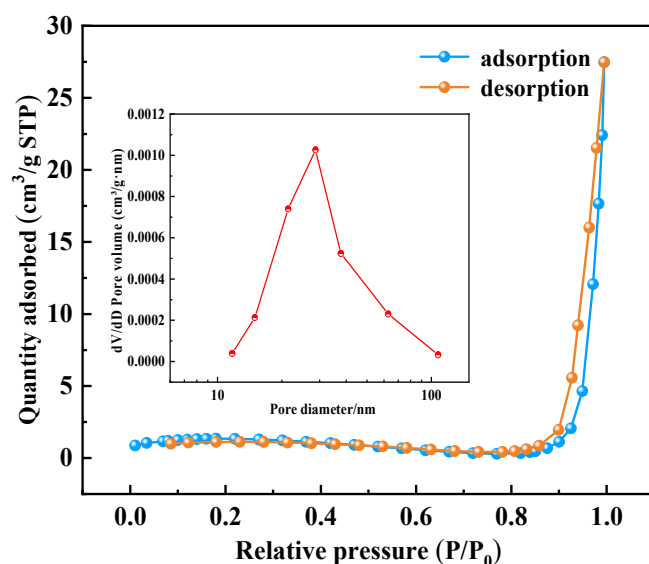


Figure 5. N₂ adsorption–desorption curve of the Ca-Ce/slag-0.8 catalyst.

3.2.3. SEM-EDS Analysis

The SEM characterized the morphologies of the Ca-Ce/slag-0.8 catalyst. As illustrated in Figure 6a, the catalyst appears as uneven and irregular strips or blocks. These strip or block structures pile on each other, with a few accumulated slit pores in between. Figure 6b depicts the images of the catalyst's local surface magnified 30,000 \times . We observed that the catalyst's surface contains some fine particles with pores. These pores facilitate efficient contact between the reactants and the active sites of the Ca-Ce/slag-0.8 catalyst.

Additionally, the EDS spectrum (Figure 6c) reflects the elemental composition and proportion of the Ca-Ce/slag-0.8 catalyst. Due to the nature of metal oxide on the steel slag carrier of the catalyst, oxygen exhibited the highest atomic percentage in the catalyst. The weight ratio of Ca and Ce was 34.82% and 34.47%, respectively, consistent with the parameter setting in the catalyst preparation, thereby confirming the homogeneity of the catalyst. Meanwhile, we identified minute amounts of Mg, Al, Si, and Cl in the catalyst, arising from the steel slag carrier.

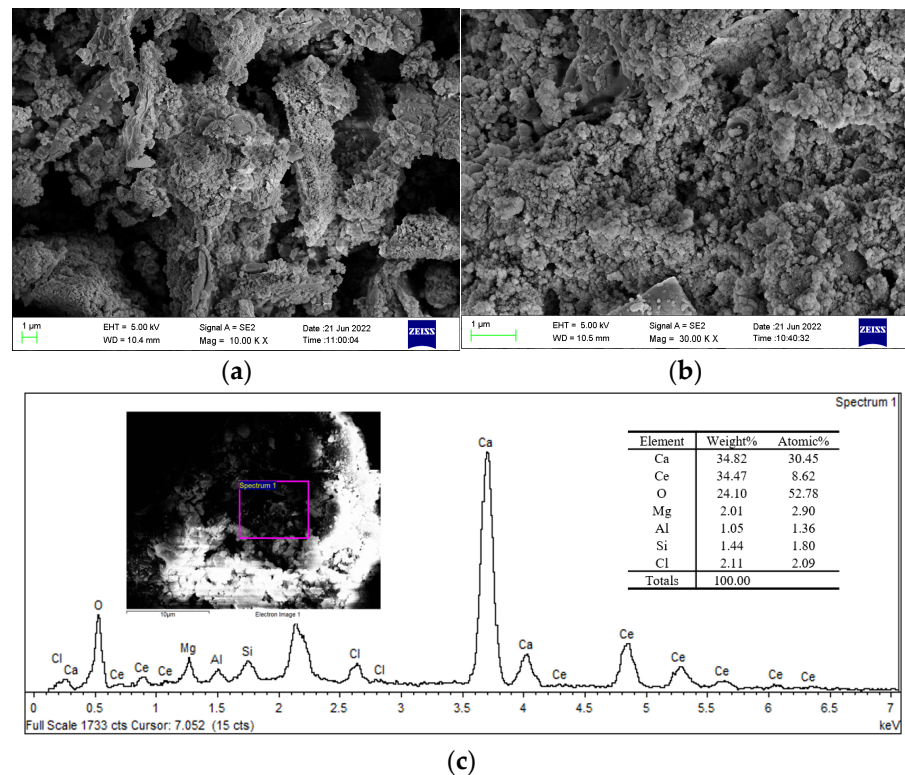


Figure 6. The SEM-EDS images of the Ca-Ce/slag-0.8 catalyst. (a) SEM image with a 10,000 \times magnification, (b) SEM image with a 30,000 \times magnification, (c) EDS element spectrum.

3.2.4. FTIR Analysis

The change in the chemical functional groups between slag and Ca-Ce/slag- x catalysts was characterized by FTIR (Figure 7). For steel slag carrier, the bands at 1435 and 875 cm^{-1} were assigned to the in-plane bending and out-of-plane bending of the carbonate groups, respectively [24]. For Ca-Ce/slag- x catalysts, a new band at 3641 cm^{-1} belonging to the stretching of the -OH groups can be observed in the FTIR spectra due to the water-absorbing characteristics of the CaO and CeO₂ components. Significantly, the -OH groups of the Ca-Ce/slag-0.8 catalyst showed a sharper band, indicating more water-absorbing potential. In addition, the bands at 800–400 cm^{-1} belonged to Ca–O and Ce–O vibration bonds.

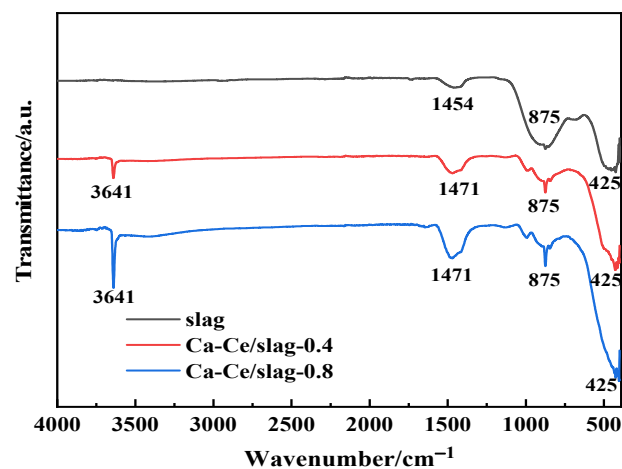


Figure 7. FTIR spectra of the slag and Ca-Ce/slag- x catalysts.

3.2.5. XPS Analysis

The XPS was deduced from a chemical state of the metal species of the Ca-Ce/slag-0.8 catalyst (Figure 8). Figure 8a shows the XPS survey with photoelectron peaks of Ce 3d, O 1s, Ca 2p, C 1s, and Si 2p at the binding energies of 930.1, 545.1, 360.1, 298.1, and 110.1 eV, respectively, reflecting the primary elements of the catalyst. Further, high-resolution XPS spectra of O 1s (Figure 8b) can be deconvoluted into two peaks. One peak centered at 531.4 eV corresponded to the oxygen species of surface hydroxyl or carbonate groups; the other peak centered at 528.7 eV was ascribed to the O^{2-} in the lattice of metal oxides [25]. Moreover, the high-resolution XPS spectra in Figure 8c confirmed the presence of Ca, evidenced by the bands assigned to Ca 2p 1/2 at 350.5 eV and Ca 2p 3/2 at 347.0 eV. Compared to the CaO peak (Ca 2p 1/2 at 349.9 eV and Ca 2p3/2 at 346.6 eV) reported in the literature, the binding energies of Ca 2p in the Ca-Ce/slag-0.8 catalyst shifted towards a higher values, suggesting the interaction between Ca and other elements (such as Ce), enhancing the stability of active components [26]. The Ce 3d spectrum of the catalyst is shown in Figure 8d. The peaks at 916.2, 907.1, 900.4, 897.8, 888.7, and 881.9 eV are typically assigned to the Ce^{4+} species. In contrast, other peaks at 902.6 and 883.9 eV were attributed to the Ce^{3+} species [27]. More Ce^{3+} species could generate more oxygen vacancies because of the unsaturated chemical bonds and charge imbalance [28], further increasing the active sites and, eventually, the activity on the catalyst. Hence, the concentration ratio of $Ce^{3+}/(Ce^{3+} + Ce^{4+})$ of the Ca-Ce/slag-0.8 catalyst was estimated as 27.9%, confirming its catalytic performance.

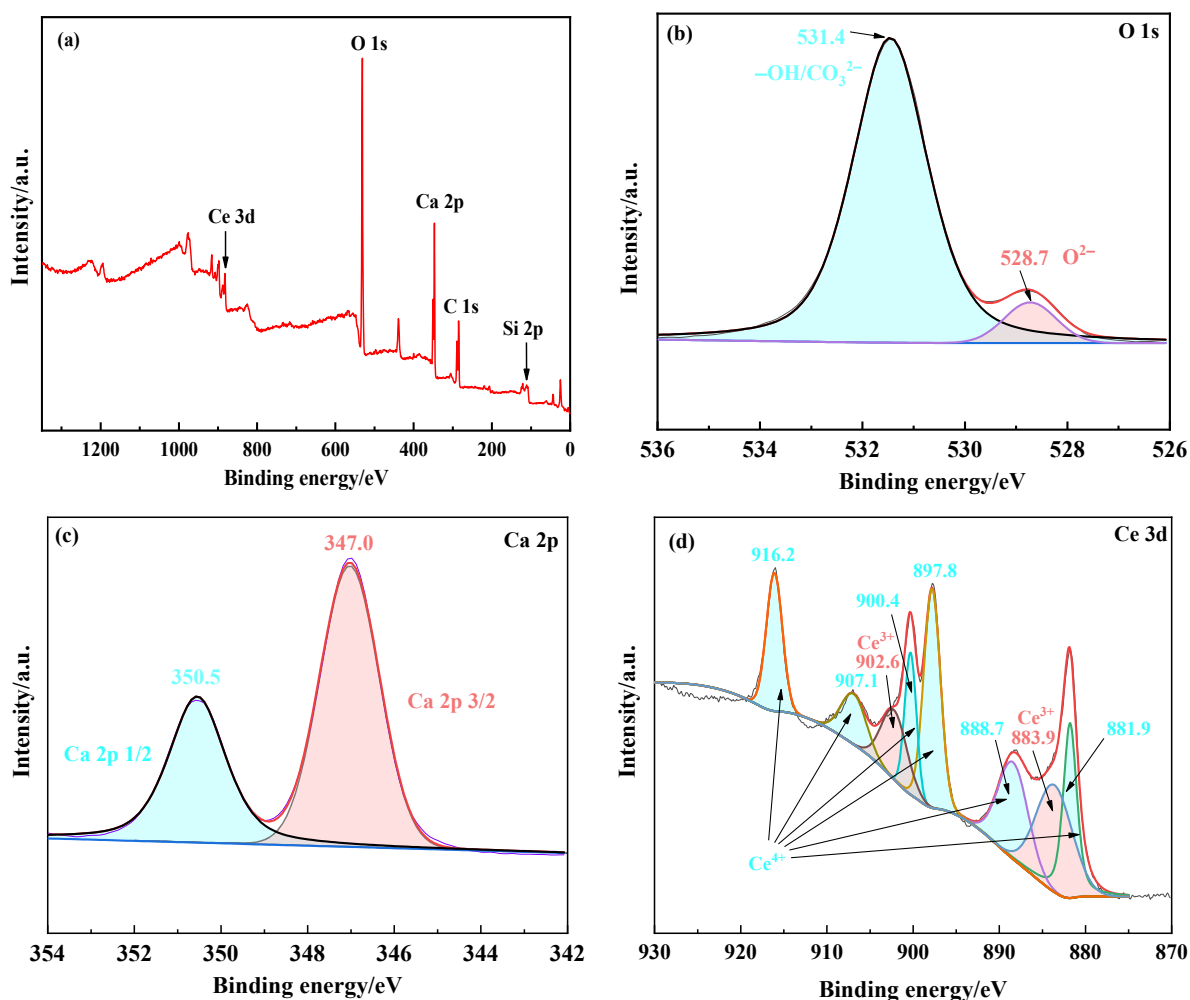


Figure 8. XPS spectra of the Ca-Ce/slag-0.8 catalyst. (a) XPS survey; (b) O 1s; (c) Ca 2p; (d) Ce 3d.

3.2.6. CO₂-TPD Analysis

The CO₂-TPD measurement studied the surface basicity of the slag and Ca-Ce/slag-*x* catalysts and the results are exhibited in Figure 9 and Table 4. Typically, surface basicity is a crucial index in determining the catalytic activity of solid base catalysts. The TPD profile of the steel slag exhibited three desorption peaks, with a basicity of 0.009, 0.110, and 0.069 mmol/g during the temperature intervals of 50–530, 530–745, and 745–900 °C, respectively. The total basicity of the slag added up to 0.188 mmol/g. It was challenging to support catalytic transesterification based on this low value. The Ca-Ce/slag-0.4 and Ca-Ce/slag-0.8 catalysts exhibited no desorption peak at 50–340 °C, demonstrating the negligible weak basic sites. For the Ca-Ce/slag-0.4 catalyst, two distinct desorption peaks were revealed at temperature intervals of 350–540 and 540–750 °C, correlating to the moderate and strong base sites, with respective basicities of 0.235 and 0.193 mmol/g. For the Ca-Ce/slag-0.8 catalyst, the corresponding temperature intervals of the moderate and strong base sites were shown at 340–560 and 560–800 °C, with corresponding basicities of 0.758 and 0.509 mmol/g. With the increased additive of active components Ca and Ce, the temperature range of desorption peaks moved to the high-temperature region, and the basicity increased correspondingly. The total basicity of the Ca-Ce/slag-0.4 and Ca-Ce/slag-0.8 catalysts was 0.445 and 1.289 mmol/g, respectively. In summary, the adequate basicity of the Ca-Ce/slag-0.8 catalyst can guarantee a high catalytic performance in transesterification. This finding compares with the HNTS-La /Ca catalyst, whose total basicity is 0.809 mmol/g [29].

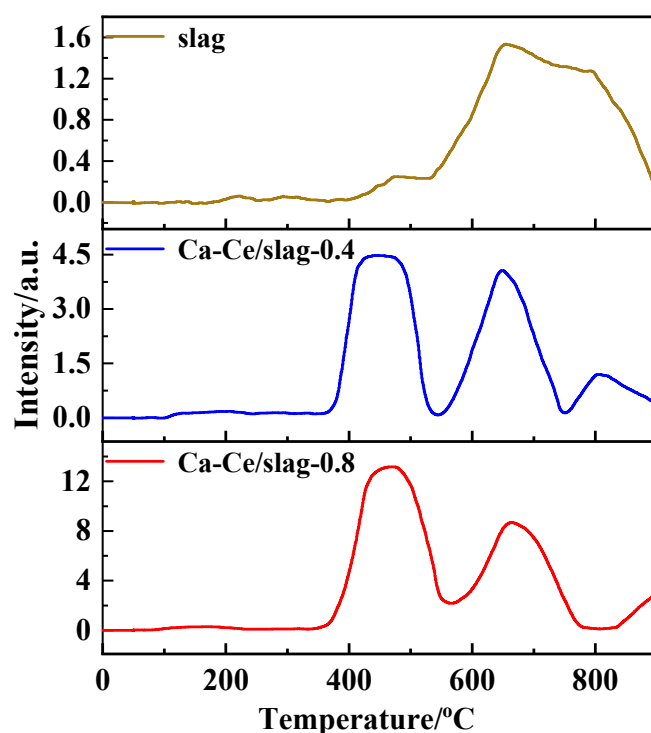


Figure 9. CO₂-TPD profiles of the slag and Ca-Ce/slag-*x* catalysts.

Table 4. CO₂-TPD data for the slag and Ca-Ce/slag-*x* catalysts.

Samples	Temperature Interval/°C	Peak Temperature/°C	Basicity/(mmol/g)	Total Basicity/(mmol/g)
Slag	50–530	476	0.009	0.188
	530–745	656	0.110	
	745–900	745	0.069	
Ca-Ce/slag-0.4	50–350	206	0.017	0.445
	350–540	446	0.235	
	540–750	649	0.193	
Ca-Ce/slag-0.8	50–340	168	0.022	1.289
	340–560	469	0.758	
	560–800	664	0.509	

3.3. Catalytic Activity

3.3.1. Transesterification Parameters Optimization

Using the Ca-Ce/slag-0.8 catalyst, the transesterification of palm oil with methanol to obtain the corresponding FAMES' yields was investigated by studying the reaction parameters: catalyst dosage, methanol-to-palm-oil molar ratio, reaction temperature, and reaction duration. The optimization results are shown in Figure 10.

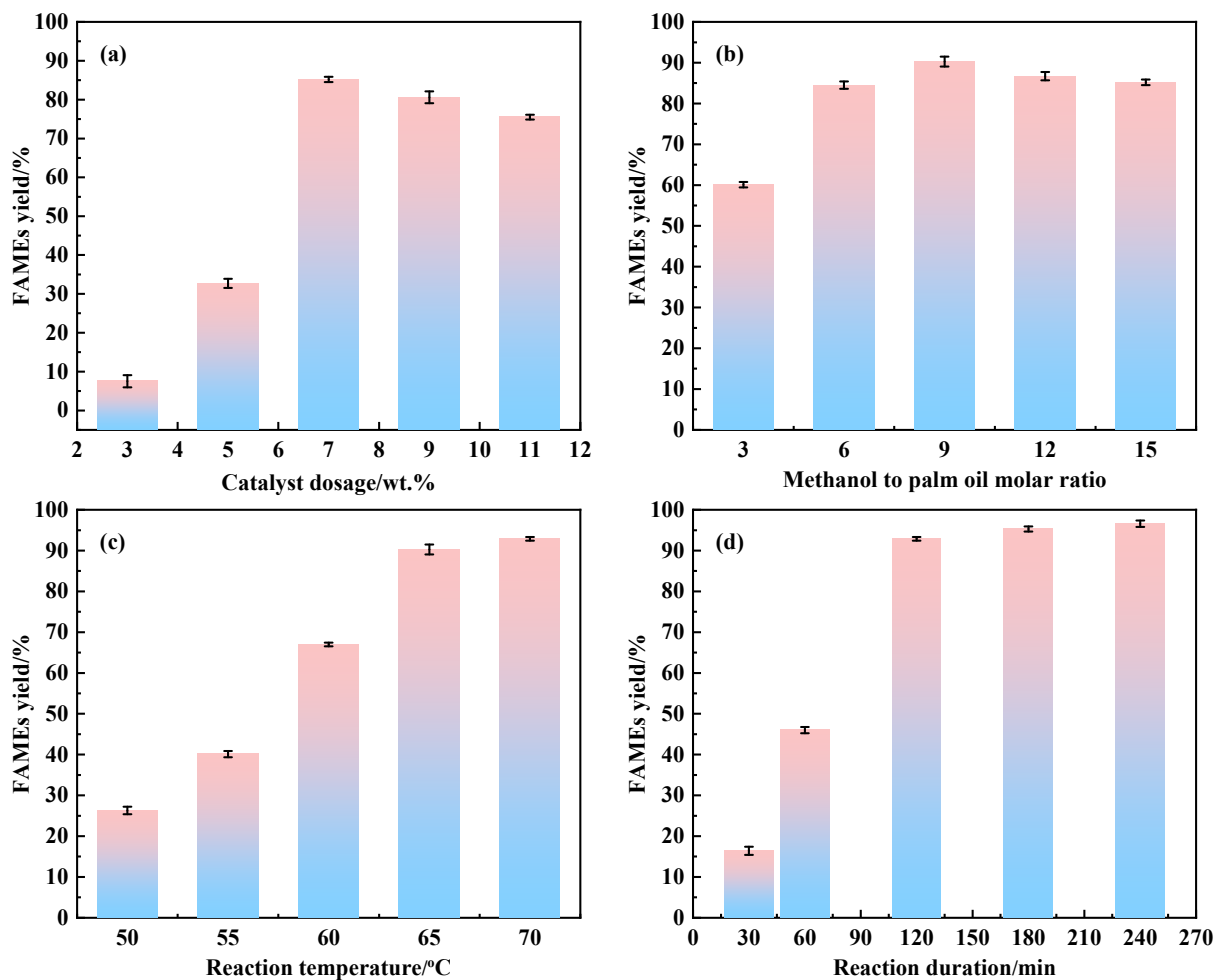


Figure 10. Effects of transesterification parameters on FAMES yield: (a) Catalyst dosage; (b) Methanol-to-palm-oil molar ratio; (c) Reaction temperature; (d) Reaction duration.

The optimization study of the catalyst dosage was performed using 3, 5, 7, 9, and 11 wt.% dosages for 120 min at 65 °C with a methanol-to-palm-oil molar ratio of 15. As

depicted in Figure 10a, the catalyst dosage dramatically affects the FAMEs yield. When the catalyst dosage was 3 wt.%, the concentration in the reaction system was sparse, making the reaction incomplete, achieving a mere 7.5% yield. The number of O^{2-} anion sites is proportional to the catalyst dosage. Higher dosages can provide more sites for adsorbing H^+ from methanol to form active centers [30], thus improving the contact of the reactants with the active centers, ultimately improving the transesterification efficiency. So, the FAMEs' yield was optimized (from 32.7%) to 85.2% as the catalyst dosage ranged from 5 to 7 wt.%. However, the yield started to decrease with further catalyst dosing. Figure 10a depicts that the FAMEs' yield depreciated to 75.5% when the catalytic dosage was further increased to 11 wt.%. This result could be attributed to excessive catalyst dosage causing saponification, affecting the main reaction's transesterification, thereby lowering the reaction yield [31]. In summary, a 7 wt.% catalyst dosage was selected as optimum.

The methanol-to-palm-oil molar ratio optimization was carried out under 3, 6, 9, 12, and 15 ratios for 120 min at 65 °C with 7 wt.% catalyst dosage. The methanol-to-oil molar ratio is vital in transesterification, where the stoichiometric ratio of transesterification between palm oil and methanol is at least 1:3 [16]. Higher positive FAMEs' yield can be obtained by increasing methanol dosage due to the reversible nature of transesterification. As shown in Figure 10b, when the molar ratio of methanol to palm oil is on a 3-to-9 scale, the increase in the molar ratio was beneficial in improving the FAMEs yield, where the FAMEs yield increased from 60.1% to 90.3%. Increasing the methanol content is conducive to reducing the viscosity of the reaction system, thereby reducing the mass transfer resistance between reactants, and further improving the conversion efficiency of reactants. However, a depressing trend of FAMEs yield was observed when the molar ratio exceeded 9. Excessive methanol lowers the contact between the catalyst and palm oil, leading to a reduced yield.

Furthermore, the reaction temperature was optimized under 50, 55, 60, 65, and 70 °C at 120 min duration using a 7 wt.% catalyst dosage and a methanol-to-palm-oil molar ratio of 9. When the temperature was held at 50 °C (Figure 10c), the reaction between methanol and palm oil in the presence of the catalyst resulted in the lowest FAMEs' yield because the temperature was lower than that required for conversion reaction into methyl ester molecules [32]. In the transesterification of macromolecular triglycerides, sufficient temperature is needed to provide enough energy to overcome the threshold. On the other hand, increasing the temperature can reduce the reactant viscosity and improve the miscibility, thus decreasing the mass-transfer resistance [33]. The FAMEs' yield increased substantially from 26.3% to 90.3% by raising the reaction temperature from 50 to 65 °C. Further increasing the reaction temperature to 70 °C improved the FAMEs yield to 92.9%. At 70 °C, the molecular movement rate of the reaction system was fast enough to enhance the effective collision chance between the reactants and the catalyst, thus obtaining a higher FAMEs' yield.

To optimize the reaction duration within 30–240 min, we set other conditions at their optimized values, i.e., 7 wt.% catalyst dosage, nine methanol-to-palm-oil molar ratio, and 70 °C. The transesterification rate is slow, especially the solid catalysts. Palm oil and methanol are immiscible, and the whole reaction system is a catalyst–methanol–palm oil three-phase state, cumbersome to homogenize. At the same time, the FAMEs' yield of transesterification was low in the initial reaction stage due to the palm oil and methanol needing to be mixed and diffused for a long duration to adsorb to the active center on the catalyst. As evidenced in Figure 10d, a 16.4% FAMEs' yield was attained after the initial 30 min of transesterification. It increased significantly to 92.9% when the reaction reached the 120 min mark. When the reaction duration was extended to 180 min, the FAMEs' yield slowly enhanced to 95.3%. After that, a puny increase of 1.3% FAMEs' yield was achieved upon increasing the duration to 240 min. We opine that the transesterification reached equilibrium when the reaction duration exceeded 180 min.

Table 5 presents the catalytic performance in the transesterification compared with some recent reports on solid base catalysts. These studies considered the production conversion (or yield) and transesterification operating parameters. A >90% conversion

or biodiesel yield was obtained from various types of solid base catalysts under different transesterification conditions. Based on the scientific literature, our results revealed that the Ca-Ce/slag-0.8 catalyst has satisfactory catalytic performance and relatively moderate transesterification conditions compared to other heterogeneous base catalysts. Moreover, the Ca-Ce/slag-0.8 catalyst optimizes the steel slag waste, saving preparation costs, and making it highly applicable industrially.

Table 5. Comparison of performance efficiencies of various base catalysts.

Catalyst	Oil Feedstock	Transesterification Parameters				Con. or Yield ⁴ /%	Ref.
		C. Dosage ¹ /wt. %	Molar Ratio ²	Temp ³ /°C	Time /min		
CaO/CeO ₂	Waste seed oil	4	9	70	90	90.14	[34]
ZnO/BiFeO ₃	Canola oil	4	15	65	360	95.43	[35]
K ₂ CO ₃ /γ-Al ₂ O ₃	Sunflower oil	5	12	80	240	99.3	[36]
Ca-Mg-Al	Sunflower oil	2.5	15	60	360	95	[30]
NaOH/Chitosan-Fe ₃ O ₄	Waste cooking oil	0.5	6	25	270	92	[37]
biochar/CaO-K ₂ CO ₃	Waste edible oil	4	18	65	200	98.83	[23]
MgO/CaO nanorods	Castor oil	6	15	70	70	96.2	[38]
CuO/ZnO	Waste cooking oil	5	9	65	120	93.5	[39]
Acai seed ash	Soybean oil	12	18	100	60	98.5	[40]
Ca-Ce/slag-0.8	Palm oil	7	9	70	180	95.3	This study

¹ C. dosage—catalyst dosage; ² Molar ratio—alcohol-to-oil molar ratio; ³ Temp—temperature; ⁴ Con. or yield—conversion or yield.

3.3.2. Effect of FFAs Content

To verify the acid resistance effect of the Ca-Ce/slag-0.8 catalyst, we added 2, 5, and 8 wt.% of oleic acid to the palm oil under optimal conditions: 7 wt.% catalyst dosage, 9 methanol-to-oil molar ratio, and reaction at 70 °C for 180 min. With 2 and 5 wt.% oleic acid added to the palm oil, the FAMES' yield decreased from 95.3% to 84.8% and 78.9%, respectively (Figure 11). However, a 63.1% FAMES' yield was still achieved even when up to 8 wt.% oleic acid was added. We found that the Ca-Ce/slag-0.8 catalyst has specific acid resistance in transesterification, but the oil's free fatty acids' content should not be higher than 5 wt.%.

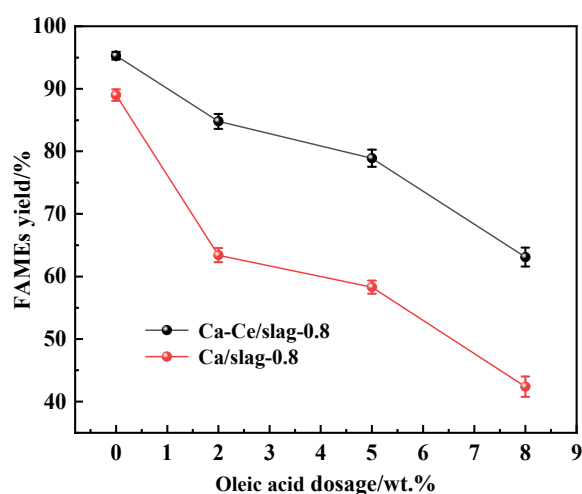


Figure 11. Effect of oleic acid dosage on the FAMES yield.

The Ca/slag-0.8 catalyst was synthesized under the same preparation conditions for comparison, and its acid resistance was studied (Figure 11). With the addition of oleic acid, the FAMES' yield of Ca/slag-0.8 catalyst decreased faster than that of the Ca-Ce/slag-0.8 catalyst. Only 42.4% of the FAMES' yield could be obtained when 8 wt.% of oleic acid was

added to the transesterification reaction. This finding indicates that the acid resistance of Ca-Ce/slag-0.8 was more enhanced than that of Ca/slag-0.8.

3.4. Catalyst Reusability

The reusability of solid catalysts is an attractive property relative to homogeneous catalysts. Transesterification was conducted at optimized conditions for three recycling tests. During each cycle, the Ca-Ce/slag-0.8 catalyst was reused by processing in two different ways: (1) Separated from the transesterification mixture by filtration and dried at 105 °C for 5 h; (2) Separated from the transesterification mixture by centrifugation and washed thrice with n-hexane to remove polar and non-polar adsorbed compounds before drying at 105 °C for 5 h. As depicted in Figure 12, for the direct drying method, the Ca-Ce/slag-0.8 catalyst exhibited good stability for the first two cycles, achieving 95.3% and 90.1% FAMES' yields. After that, the yield depreciated with the recycling number. Only 82.1% of the FAMES' yield was achieved in the third cycle. In contrast, the FAMES' yield slowly decreased from 95.3% to 93.8%, and 91.2% after the three cycles, with the one washed with n-hexane. This observation indicated that the active site on the catalyst was covered by organic matter, which hindered the catalytic activity of the Ca-Ce/slag-0.8. Lee et al. [41] reported that the palm oil conversion was reduced to 70% after the third cycles catalyzed by waste obtuse horn shell-derived CaO catalyst. In summary, the Ca-Ce/slag-0.8 catalyst synthesized in the present study exhibited an appreciable FAMES' yield.

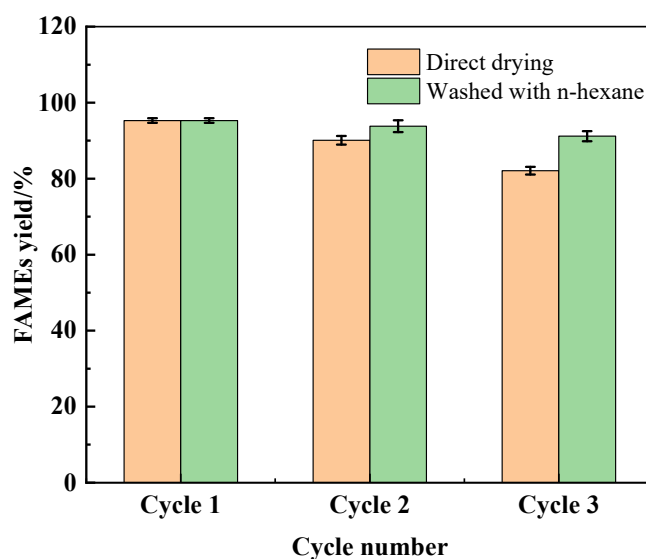


Figure 12. Effect of recycling of the Ca-Ce/slag-0.8 catalyst on the FAMES' yield.

4. Discussion

This study synthesized a newly cost-effective base catalyst of Ca-Ce/slag to generate biodiesel from palm oil. The effect of the mass ratio of Ca-Ce to steel slag on the transesterification activity was investigated. Moreover, diversified characterization techniques were employed to analyze the catalyst properties (such as crystalline phases, microscopic pore structure, morphology, functional groups, and surface basicity). The results showed that the mass ratio of Ca-Ce to steel slag at 0.8 (i.e., Ca-Ce/slag-0.8 catalyst) exhibited excellent physical and chemical properties. According to the range of transesterification conditions selected in this study, the optimal transesterification conditions are as follows: methanol: oil molar ratio of 9, catalyst dosage of 7 wt.%, and reaction at 70 °C for 180 min, yielding 95.3% of FAMES. Moreover, the Ca-Ce/slag-0.8 catalyst exhibited stable catalytic performance after three cycles with >90% FAMES' yield. Consequently, this study provides a new view on the resource utilization of steel slag and an excellent prospect for developing low-cost solid biodiesel catalysts.

Author Contributions: Conceptualization, J.S. and H.Y.; methodology, G.Q.; software, G.Q. and P.Z.; validation, P.Z., J.S. and X.C.; formal analysis, X.L.; investigation, H.Y.; resources, J.S.; data curation, H.Y.; writing—original draft preparation, H.S.; writing—review and editing, J.S.; visualization, H.S.; supervision, X.C.; project administration, H.Y. and H.S.; funding acquisition. All authors have read and agreed to the published version of the manuscript.

Funding: This research was funded by Open Project of Shandong Key Laboratory of Biomass Gasification Technology [BG-KFX-08], the National Natural Science Foundation of China [52206262], the Science, Education and Industry Training New Project of Qilu University of Technology [2022PX091], the Natural Science Foundation of Shandong Province, China [ZR2020QE210], “20 New Universities” Funding Project of Jinan [2021GXRC053] and Undergraduate Training Program for Innovation and Entrepreneurship Program of Shandong Province.

Data Availability Statement: The data that support the findings of this study are available within the article.

Conflicts of Interest: The authors declare no conflict of interest.

References

1. Woranuch, W.; Ngaosuwan, K.; Kiatkittipong, W.; Wongsawaeng, D.; Appamana, W.; Powell, J.; Rokhum, S.L.; Assabumrungrat, S. Fine-tuned fabrication parameters of CaO catalyst pellets for transesterification of palm oil to biodiesel. *Fuel* **2022**, *323*, 124356. [[CrossRef](#)]
2. Li, H.; Wang, Y.; Ma, X.; Guo, M.; Li, Y.; Li, G.; Cui, P.; Zhou, S.; Yu, M. Synthesis of CaO/ZrO₂ based catalyst by using UiO-66(Zr) and calcium acetate for biodiesel production. *Renew. Energy* **2022**, *185*, 970–977. [[CrossRef](#)]
3. Zul, N.A.; Ganesan, S.; Hamidon, T.S.; Oh, W.D.; Hussin, M.H. A review on the utilization of calcium oxide as a base catalyst in biodiesel production. *J. Environ. Chem. Eng.* **2021**, *9*, 105741. [[CrossRef](#)]
4. Yaşar, F. Biodiesel production via waste eggshell as a low-cost heterogeneous catalyst: Its effects on some critical fuel properties and comparison with CaO. *Fuel* **2019**, *255*, 115821–115828. [[CrossRef](#)]
5. Teo, S.H.; Rashid, U.; Taufiq-Yap, Y.H. Heterogeneous catalysis of transesterification of jatropha curcas oil over calcium-cerium bimetallic oxide catalyst. *RSC. Adv.* **2014**, *4*, 48836–48847. [[CrossRef](#)]
6. Pandit, P.R.; Fulekar, M.H. Biodiesel production from microalgal biomass using CaO catalyst synthesized from natural waste material. *Renew. Energy* **2019**, *136*, 837–845. [[CrossRef](#)]
7. Dehghani, S.; Haghighi, M.; Vardast, N. Structural/texture evolution of CaO/MCM nanocatalyst by doping various amounts of cerium for active and stable catalyst: Biodiesel production from waste vegetable cooking oil. *Int. J. Energy. Res.* **2019**, *43*, 3779–3793. [[CrossRef](#)]
8. Zhang, N.; Xue, H.; Hu, R. The activity and stability of CeO₂@CaO catalysts for the production of biodiesel. *RSC. Adv.* **2018**, *8*, 32922. [[CrossRef](#)]
9. Shu, K.; Sasaki, K. Occurrence of steel converter slag and its high value-added conversion for environmental restoration in China: A review. *J. Clean. Prod.* **2022**, *373*, 133876. [[CrossRef](#)]
10. Gan, Y.; Li, C.; Ke, W.; Deng, Q.; Yu, T. Study on pavement performance of steel slag asphalt mixture based on surface treatment. *Case. Stud. Constr. Mat.* **2022**, *16*, e1131. [[CrossRef](#)]
11. Song, B.; Wang, Z.; Li, J.; Ma, Y. Preparation and electrocatalytic properties of kaolin/steel slag particle electrodes. *Catal. Commun.* **2021**, *148*, 106177. [[CrossRef](#)]
12. Liu, G.; Yang, J.; Xu, X. Synthesis of hydrotalcite-type mixed oxide catalysts from waste steel slag for transesterification of glycerol and dimethyl carbonate. *Sci. Rep-UK* **2020**, *10*, 10273. [[CrossRef](#)]
13. Casiello, M.; Losito, O.; Aloia, A.; Caputo, D.; Fusco, C.; Attrotto, R.; Monopoli, A.; Nacci, A.; D’Accolti, L. Steel Slag as New Catalyst for the Synthesis of Fames from Soybean Oil. *Catalyst* **2021**, *11*, 619. [[CrossRef](#)]
14. Kang, L.; Zhang, Y.J.; Zhang, L.; Zhang, K. Preparation, characterization and photocatalytic activity of novel CeO₂ loaded porous alkali-activated steel slag-based binding material. *Int. J. Hydrogen. Energy.* **2017**, *42*, 17341–17349. [[CrossRef](#)]
15. Lin, S.; Zhang, T.; Cao, X.; Liu, X. Recovery of converter steel slag to prepare catalytic H₂O₂ degradation of dye wastewater as a catalyst. *J. Mater. Sci-Mater. El.* **2021**, *32*, 24889–24901. [[CrossRef](#)]
16. Gao, L.; Teng, G.; Xiao, G.; Wei, R. Biodiesel from palm oil via loading KF/Ca–Al hydrotalcite catalyst. *Biomass Bioenergy* **2010**, *34*, 1283–1288. [[CrossRef](#)]
17. Kesserwan, F.; Ahmad, M.N.; Khalil, M.; El-Rassy, H. Hybrid CaO/Al₂O₃ aerogel as heterogeneous catalyst for biodiesel production. *Chem. Eng. J.* **2020**, *385*, 123834. [[CrossRef](#)]
18. Borah, M.J.; Das, A.; Das, V.; Bhuyan, N.; Deka, D. Transesterification of waste cooking oil for biodiesel production catalyzed by Zn substituted waste egg shell derived CaO nanocatalyst. *Fuel* **2019**, *242*, 345–354. [[CrossRef](#)]
19. Ning, Y.; Niu, S. Preparation and catalytic performance in esterification of a bamboo-based heterogeneous acid catalyst with microwave assistance. *Energy Convers. Manag.* **2017**, *153*, 446–454. [[CrossRef](#)]

20. Qu, T.; Niu, S.; Zhang, X.; Han, K.; Lu, C. Preparation of calcium modified Zn-Ce/Al₂O₃ heterogeneous catalyst for biodiesel production through transesterification of palm oil with methanol optimized by response surface methodology. *Fuel* **2021**, *284*, 118986. [[CrossRef](#)]
21. Yadav, M.; Sharma, Y.C. Process optimization and catalyst poisoning study of biodiesel production from kusum oil using potassium aluminum oxide as efficient and reusable heterogeneous catalyst. *J. Clean. Prod.* **2018**, *199*, 593–602. [[CrossRef](#)]
22. Zhang, Y.; Niu, S.; Kan, H.; Li, Y.; Lu, C. Synthesis of the SrO–CaO–Al₂O₃ trimetallic oxide catalyst for transesterification to produce biodiesel. *Renew. Energy* **2021**, *168*, 981–990.
23. Foroutan, R.; Mohammadi, R.; Razeghi, J.; Ramavandi, B. Biodiesel production from edible oils using algal biochar/CaO/K₂CO₃ as a heterogeneous and recyclable catalyst. *Renew. Energy* **2021**, *168*, 1207–1216. [[CrossRef](#)]
24. Murguía-Ortiz, D.; Cordova, I.; Manriquez, M.E.; Ortiz-Islas, E.; Cabrera-Sierra, R.; Contreras, J.L.; Alcantar-Vazquez, B.; Trejo-Rubio, M.; Vazquez-Rodriguez, J.T.; Castro, L.V. Na-CaO/MgO dolomites used as heterogeneous catalysts in canola oil transesterification for biodiesel production. *Mater. Lett.* **2021**, *291*, 129587. [[CrossRef](#)]
25. Niu, S.; Zhang, X.; Ning, Y.; Zhang, Y.; Qu, T.; Hu, X.; Gong, Z.; Lu, C. Dolomite incorporated with cerium to enhance the stability in catalyzing transesterification for biodiesel production. *Renew. Energy* **2020**, *154*, 107–116. [[CrossRef](#)]
26. Wang, J.; Yang, L.; Luo, W.; Yang, G.; Miao, C.; Fu, J.; Xing, S.; Fan, P.; Lv, P.; Wang, Z. Sustainable biodiesel production via transesterification by using recyclable Ca₂MgSi₂O₇ catalyst. *Fuel* **2017**, *196*, 306–313. [[CrossRef](#)]
27. Ma, S.; Tan, H.; Li, Y.; Wang, P.; Zhu, Y. Excellent low-temperature NH₃-SCR NO removal performance and enhanced H₂O resistance by Ce addition over the Cu_{0.02}Fe_{0.2}Ce_yTi_{1-y}O_x (y = 0.1, 0.2, 0.3) catalysts. *Chemosphere* **2019**, *243*, 125309. [[CrossRef](#)]
28. Ma, Y.; Li, W.; Wang, H.; Chen, J.; Wen, J.; Xu, S.; Tian, X.; Gao, L.; Hou, Z.; Zhang, Q. Enhanced performance of iron-cerium NO_x reduction catalysts by sulfuric acid treatment: The synergistic effect of surface acidity and redox capacity. *Appl. Catal. A-Gen.* **2021**, *621*, 118200. [[CrossRef](#)]
29. Lin, T.; Zhao, S.; Niu, S.; Lyu, Z.; Hu, X. Halloysite nanotube functionalized with La-Ca bimetallic oxides as novel transesterification catalyst for biodiesel production with molecular simulation. *Energy Convers. Manag.* **2020**, *220*, 113138. [[CrossRef](#)]
30. Dahdah, E.; Estephane, J.; Haydar, R.; Youssef, Y.; Khoury, B.E.; Gennequin, C.; Aboukais, A.; Abi-Aad, E.; Aouad, S. Biodiesel production from refined sunflower oil over Ca–Mg–Al catalysts: Effect of the composition and the thermal treatment. *Renew. Energy* **2020**, *146*, 1242–1248. [[CrossRef](#)]
31. Li, H.; Niu, S.; Lu, C.; Liu, M.; Huo, M. Transesterification catalyzed by industrial waste—Lime mud doped with potassium fluoride and the kinetic calculation. *Energy Convers. Manag.* **2014**, *86*, 1110–1117. [[CrossRef](#)]
32. Al-Muhtaseb, A.H.; Osman, A.I.; Jamil, F.; Mehta, N.; Al-Haj, L.; Coulon, F.; Al-Maawali, S.; Al Nabhani, A.; Kyaw, H.H.; Myint, M.T.Z.; et al. Integrating life cycle assessment and characterisation techniques: A case study of biodiesel production utilising waste Prunus Armeniaca seeds (PAS) and a novel catalyst. *J. Environ. Manag.* **2022**, *304*, 114319. [[CrossRef](#)]
33. Farooq, M.; Ramli, A.; Naeem, A. Biodiesel production from low FFA waste cooking oil using heterogeneous catalyst derived from chicken bones. *Renew. Energy* **2015**, *76*, 362–368. [[CrossRef](#)]
34. Al-Muhtaseb, A.H.; Osman, A.I.; Kumar, P.S.M.; Jamil, F.; Al-Haj, L.; Al Nabhani, A.; Kyaw, H.H.; Myint, M.T.Z.; Mehta, N.; Rooney, D.W. Circular economy approach of enhanced bifunctional catalytic system of CaO/CeO₂ for biodiesel production from waste loquat seed oil with life cycle assessment study. *Energy Convers. Manag.* **2021**, *236*, 114040. [[CrossRef](#)]
35. Salimi, Z.; Hosseini, S.A. Study and optimization of conditions of biodiesel production from edible oils using ZnO/BiFeO₃ nano magnetic catalyst. *Fuel* **2019**, *239*, 1204–1212. [[CrossRef](#)]
36. Junior, E.S.; Perez, V.H.; Reyero, I.; Serrano-Lotina, A.; Justo, O.R. Biodiesel production from heterogeneous catalysts based K₂CO₃ supported on extruded γ-Al₂O₃. *Fuel* **2019**, *241*, 311–318. [[CrossRef](#)]
37. Helmi, M.; Hemmati, A. Synthesis of magnetically solid base catalyst of NaOH/Chitosan-Fe₃O₄ for biodiesel production from waste cooking oil: Optimization, kinetics and thermodynamic studies. *Energy Convers. Manag.* **2021**, *248*, 114807. [[CrossRef](#)]
38. Abukhadra, M.R.; Mohamed, A.S.; El-Sherbeeney, A.M.; Soliman, A.T.A.; Elgawad, A.E.E.A. Sonication induced transesterification of castor oil into biodiesel in the presence of MgO/CaO nanorods as a novel basic catalyst: Characterization and optimization. *Chem. Eng. Process.* **2020**, *154*, 108024. [[CrossRef](#)]
39. Guo, M.; Jiang, W.; Ding, J.; Lu, J. Highly active and recyclable CuO/ZnO as photocatalyst for transesterification of waste cooking oil to biodiesel and the kinetics. *Fuel* **2022**, *315*, 123254. [[CrossRef](#)]
40. Mares, E.K.L.; Gonçalves, M.A.; Lourenço, E.K.; Luz, P.T.S.; Filho, G.N.R.; Zamian, J.R.; Conceição, L.R.V. Acai seed ash as a novel basic heterogeneous catalyst for biodiesel synthesis: Optimization of the biodiesel production process. *Fuel* **2021**, *299*, 120887. [[CrossRef](#)]
41. Lee, S.L.; Wong, Y.C.; Tan, Y.P.; Yew, S.Y. Transesterification of palm oil to biodiesel by using waste obtuse horn shell-derived CaO catalyst. *Energy Convers. Manag.* **2015**, *93*, 282–288. [[CrossRef](#)]

Disclaimer/Publisher’s Note: The statements, opinions and data contained in all publications are solely those of the individual author(s) and contributor(s) and not of MDPI and/or the editor(s). MDPI and/or the editor(s) disclaim responsibility for any injury to people or property resulting from any ideas, methods, instructions or products referred to in the content.